Eur. Phys. J. C 55, 409–415 (2008)
DOI 10.1140/epjc/s10052-008-0605-7

THE EUROPEAN PHYSICAL JOURNAL C

Regular Article – Theoretical Physics

Meson and tetra-quark mixing

Ping Wang[1,2], Stephen R. Cotanch[1], Ignacio J. General[3,a]

[1] Department of Physics, North Carolina State University, Raleigh, NC 27695-8202, USA
[2] Jefferson Laboratory, 12000 Jefferson Ave., Newport News, VA 23606, USA
[3] Bayer School of Natural and Environmental Sciences, Duquesne University, 600 Forbes Ave., Pittsburgh, PA 15282, USA

Received: 31 January 2008 / Revised version: 29 March 2008 /
Published online: 7 May 2008 –

Abstract. The mixing between $q\bar{q}$ meson and $q\bar{q}q\bar{q}$ tetra-quark states is examined within an effective QCD Coulomb gauge Hamiltonian model. Mixing matrix elements of the Hamiltonian are computed and then diagonalized yielding an improved prediction for the low-lying $J^{PC} = 0^{\pm+}, 1^{--}$ isoscalar spectra. Mixing effects were found significant for the scalar hadrons but not for the 1^{--} states, which is consistent with the ideal mixing of vector mesons. A perturbative assessment of the exact QCD kernel is also reported.

PACS. 12.39.Mk; 12.39.Pn; 12.39.Ki; 12.40.Yx

1 Introduction

Hadronic structure remains an interesting but challenging problem. This is because quantum chromodynamics (QCD) permits a variety of hadron formations such as $q\bar{q}$ mesons, $q\bar{q}q\bar{q}$ tetra-quarks, $q\bar{q}g$ hybrids and gg glueballs. These states will, in general, also mix via quark pair annihilation/formation, which further complicates this issue. Unfortunately experimental information [1] is predominantly limited to masses, widths and spectroscopic quantum numbers providing us with little insight of the structure. Accordingly, theoretical input is needed and this paper reports a consistent model study of the dynamic mixing between $q\bar{q}$ meson and $q\bar{q}q\bar{q}$ tetra-quark states.

There are abundant mixing analyses in the literature involving mesons, glueballs and hybrids utilizing a variety of methods including perturbation theory, relativistic Feynman–Schwinger path integrals for Green's functions [2], instantons [3], lattice QCD [4] and effective chiral approaches [5]. There have also been several meson–glueball [6–9] and quarkonia–glueball-hybrid [10, 11] phenomenological mixing studies in which the interactions are modeled, or simply parameterized, and then diagonalized to obtain relations between primitive and physical masses.

Central to this work is the mixing between meson and tetra-quark states. Published studies include two diquark, anti-diquark cluster applications with tetra-quark mixings between either hybrid [12] or quarkonium [13] states, a meson–meson coupled-channels scattering calculation [14, 15] and a quark model mixing study [16] that obtained an improved scalar spectrum by adjusting phenomenological parameters. Further, light scalar states below 1 GeV were studied in an effective Lagrangian framework [17], where it was found that the tetra-quark picture was favored over the conventional $q\bar{q}$ one; scalars with a mass larger than 1 GeV were treated as conventional $q\bar{q}$ states [18]. Certain puzzling features in this picture, such as the mass spectrum level order and decay widths, can be resolved by mixing between the p-wave $q\bar{q}$ and tetra-quark states [18, 19].

As detailed in this paper, meson–tetra-quark mixing is fundamentally due to $q\bar{q}$ pair annihilation/formation and entails the strong confining interaction. We include this mechanism using our Coulomb gauge (CG) model, which has been successfully applied to meson, glueball, hybrid and tetra-quark states [20–27]. The model Hamiltonian is obtained from the QCD Coulomb gauge Hamiltonian using a few simplifications (see below). In this way, the original non-perturbative confining interaction can be rearranged into a calculable effective potential between color densities. We utilize many-body techniques and relativistic field theory in which the non-perturbative vacuum is described as a coherent BCS ground state with quark and gluon Cooper pairs (condensates). The resulting model retains the key QCD elements and is thus capable of reasonable predictions as comprehensively documented in numerous publications [20–27]. In particular, our RPA treatment of the CG model is rigorously equivalent to the established, phenomenologically successful Schwinger–Dyson method (see [28, 29] and references therein) in the instantaneous kernel approximation.

We only focus on the mixing between $q\bar{q}$ and $q\bar{q}q\bar{q}$ configurations and, for two reasons, omit $q\bar{q}g$ hybrid and gg glueball states. First, we are interested in low-mass spectra, in which energy level mixing arguments imply that the effects from glueballs and hybrid mesons should not

[a] e-mail: ijgeneral@gmail.com

be large since these exotic hadrons have somewhat heavier masses. Indeed, in our previous model applications (and others including lattice results) the lightest hybrid and glueball masses are predicted to be slightly above [20, 21] and below [25] 2 GeV, respectively. This is in contrast to tetra-quark masses, which, due to four different color configurations, can be much lighter. In particular, we calculated [20, 22] the lightest tetra-quark to be in the color singlet–singlet state with mass closer to 1 rather than 2 GeV. The other reason for omitting quark-hybrid and quark–glueball mixing matrix elements is that for our model Hamiltonian (see Sect. 4) the former are perturbative, and thus they are expected to be weak, while the latter entirely vanish (mixing must proceed via higher order intermediate states). This would also suggest that glueball widths might not be large, as typically expected, perhaps even narrow, consistent with a recent theoretical prediction [30]. The issue of mixing involving gluonic states, however, merits a further study, which we plan to address in a separate communication.

This paper is organized into seven sections. In the next section we detail the QCD Coulomb gauge Hamiltonian and then, in Sect. 3, present a perturbative analysis of the exact Coulomb kernel. This motivates our Coulomb gauge model Hamiltonian described in Sect. 4. Meson and tetra-quark mixing is treated in Sect. 5 with numerical results given in Sect. 6. Finally, key findings and conclusions are summarized in Sect. 7.

2 QCD Coulomb gauge Hamiltonian

The exact QCD Hamiltonian in the Coulomb gauge [31] is (summation over repeated indices is used throughout)

$$H_{\rm QCD} = H_q + H_g + H_{qg} + H_{\rm C}\,, \tag{1}$$

$$H_q = \int {\rm d}\mathbf{x}\Psi^\dagger(\mathbf{x})[-{\rm i}\alpha\cdot\nabla+\beta m]\Psi(\mathbf{x})\,, \tag{2}$$

$$H_g = \frac{1}{2}\int {\rm d}\mathbf{x}\left[\mathcal{J}^{-1}\mathbf{\Pi}^a(\mathbf{x})\cdot\mathcal{J}\mathbf{\Pi}^a(\mathbf{x}) + \mathbf{B}^a(\mathbf{x})\cdot\mathbf{B}^a(\mathbf{x})\right], \tag{3}$$

$$H_{qg} = g\int {\rm d}\mathbf{x}\mathbf{J}^a(\mathbf{x})\cdot\mathbf{A}^a(\mathbf{x})\,, \tag{4}$$

$$H_{\rm C} = -\frac{g^2}{2}\int {\rm d}\mathbf{x}\,{\rm d}\mathbf{y}\mathcal{J}^{-1}\rho^a(\mathbf{x})K^{ab}(\mathbf{x},\mathbf{y})\mathcal{J}\rho^b(\mathbf{y})\,, \tag{5}$$

where g is the QCD coupling constant, Ψ is the quark field with current quark mass m, $A^a=(\mathbf{A}^a, A_0^a)$ are the gluon fields satisfying the transverse gauge condition, $\nabla\cdot\mathbf{A}^a=0$ $(a=1,2,\ldots 8)$, $\mathbf{\Pi}^a=-\mathbf{E}^a_{tr}$ are the conjugate momenta and

$$\mathbf{E}^a_{tr} = -\dot{\mathbf{A}}^a + g(1-\nabla^{-2}\nabla\nabla\cdot)f^{abc}A_0^b\mathbf{A}^c\,, \tag{6}$$

$$\mathbf{E}^a = -\dot{\mathbf{A}}^a - \nabla A_0^a + gf^{abc}A_0^b\mathbf{A}^c\,, \tag{7}$$

$$\mathbf{B}^a = \nabla\times\mathbf{A}^a + \frac{1}{2}gf^{abc}\mathbf{A}^b\times\mathbf{A}^c\,, \tag{8}$$

are the non-abelian chromodynamic fields. The color densities, $\rho^a(\mathbf{x})$, and quark currents, $\mathbf{J}^a$, are

$$\rho^a(\mathbf{x}) = \Psi^\dagger(\mathbf{x})T^a\Psi(\mathbf{x}) + f^{abc}\mathbf{A}^b(\mathbf{x})\cdot\mathbf{\Pi}^c(\mathbf{x})\,, \tag{9}$$

$$\mathbf{J}^a = \Psi^\dagger(\mathbf{x})\alpha T^a\Psi(\mathbf{x})\,, \tag{10}$$

with the standard SU(3) color matrices $T^a=\frac{\lambda^a}{2}$ and structure constants f^{abc}. The Faddeev–Popov determinant, $\mathcal{J}=\det(\mathcal{M})$, of the matrix $\mathcal{M}=\nabla\cdot\mathbf{D}$ with covariant derivative $\mathbf{D}^{ab}=\delta^{ab}\nabla - gf^{abc}\mathbf{A}^c$, is a measure of the gauge manifold curvature, and the kernel in (5) is given by $K^{ab}(\mathbf{x},\mathbf{y})=\langle\mathbf{x},a|\mathcal{M}^{-1}\nabla^2\mathcal{M}^{-1}|\mathbf{y},b\rangle$. The Coulomb gauge Hamiltonian is renormalizable, permits resolution of the Gribov problem, preserves rotational invariance, avoids spurious retardation corrections, aids identification of dominant, low-energy potentials and introduces only physical degrees of freedom (no ghosts) [32].

The bare parton fields have the normal mode expansions (bare quark spinors u, v, helicity, $\lambda=\pm1$, and color vectors $\hat{\epsilon}_{\mathcal{C}=1,2,3}$)

$$\Psi(\mathbf{x}) = \int\frac{{\rm d}\mathbf{k}}{(2\pi)^3}\Psi_{\mathcal{C}}(\mathbf{k}){\rm e}^{{\rm i}\mathbf{k}\cdot\mathbf{x}}\hat{\epsilon}_{\mathcal{C}}\,, \tag{11}$$

$$\Psi_{\mathcal{C}}(\mathbf{k}) = u_\lambda(\mathbf{k})b_{\lambda\mathcal{C}}(\mathbf{k}) + v_\lambda(-\mathbf{k})\,{\rm d}^\dagger_{\lambda\mathcal{C}}(-\mathbf{k})\,, \tag{12}$$

$$\mathbf{A}^a(\mathbf{x}) = \int\frac{{\rm d}\mathbf{k}}{(2\pi)^3}\frac{1}{\sqrt{2k}}[\mathbf{a}^a(\mathbf{k}) + \mathbf{a}^{a\dagger}(-\mathbf{k})]{\rm e}^{{\rm i}\mathbf{k}\cdot\mathbf{x}}\,, \tag{13}$$

$$\mathbf{\Pi}^a(\mathbf{x}) = -{\rm i}\int\frac{{\rm d}\mathbf{k}}{(2\pi)^3}\sqrt{\frac{k}{2}}[\mathbf{a}^a(\mathbf{k}) - \mathbf{a}^{a\dagger}(-\mathbf{k})]{\rm e}^{{\rm i}\mathbf{k}\cdot\mathbf{x}}\,, \tag{14}$$

with the Coulomb gauge transverse condition, $\mathbf{k}\cdot\mathbf{a}^a(\mathbf{k}) = (-1)^\mu k_\mu a^a_{-\mu}(\mathbf{k}) = 0$. Here $b_{\lambda\mathcal{C}}(\mathbf{k})$, $d_{\lambda\mathcal{C}}(-\mathbf{k})$ and $a^a_\mu(\mathbf{k})$ $(\mu = 0,\pm1)$ are the bare quark, anti-quark and gluon Fock operators, the latter satisfying the transverse commutation relations

$$\left[a^a_\mu(\mathbf{k}), a^{b\dagger}_{\mu'}(\mathbf{k}')\right] = (2\pi)^3\delta_{ab}\delta^3(\mathbf{k}-\mathbf{k}')D_{\mu\mu'}(\mathbf{k})\,, \tag{15}$$

with

$$D_{\mu\mu'}(\mathbf{k}) = \delta_{\mu\mu'} - (-1)^\mu\frac{k_\mu k_{-\mu'}}{k^2}\,. \tag{16}$$

3 Perturbative expansion

Before addressing meson and tetra-quark mixing, we first report a perturbative study of the kernel $K^{ab}(\mathbf{x},\mathbf{y})$. Expanding in powers of g yields

$$\mathcal{M}^{-1}\nabla^2\mathcal{M}^{-1} = \nabla^{-2} + 2g\nabla^{-2}\mathcal{A}\nabla^{-2} + 3g^2\nabla^{-2}\mathcal{A}\nabla^{-2}\mathcal{A}\nabla^{-2} + \ldots\,, \tag{17}$$

where $\mathcal{A}^{ab}=f^{abc}\mathbf{A}^c\cdot\nabla$. Note that the first term represents the simple, long-ranged Coulomb interaction. We have perturbatively calculated the expectation value of the Hamiltonian component with this kernel for 0^{++} $q\bar{q}$ states (the Faddeev–Popov terms are also included):

$$E_{\rm C} \equiv \left\langle\Psi^{JPC}|H_{\rm C}|\Psi^{JPC}\right\rangle = g^2E_2^{\rm C} + g^4E_4^{\rm C} + g^6E_6^{\rm C} + \ldots$$

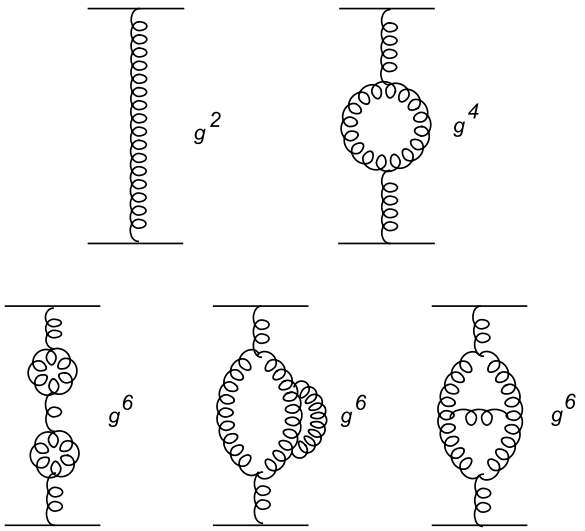

Fig. 1. Diagrams for the kernel expansion to order g^6

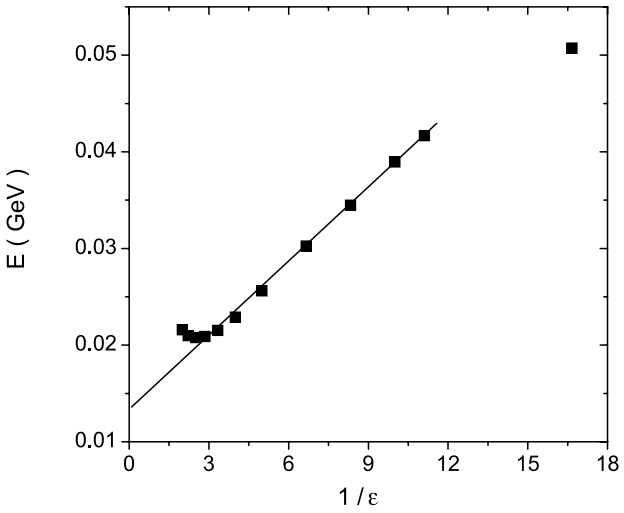

Fig. 2. The interaction energy to order g^4 vs. $1/\epsilon$

In this paper all wavefunction kets, $|\psi\rangle$, have unit norm. The leading diagrams corresponding to g^2, g^4 and g^6 are shown in Fig. 1. The g^2 diagram contributes

$$E_2^{\mathrm{C}} = \int \mathrm{d}\mathbf{q}\mathrm{d}\mathbf{q}' \frac{\mathcal{F}(\mathbf{q},\mathbf{q}')}{\mathbf{p}^2}\,,$$
$$\mathcal{F} = \mathcal{U}^\dagger_{\lambda_1}(\mathbf{q})\mathcal{U}_{\lambda_1'}(\mathbf{q}')\mathcal{V}^\dagger_{\lambda_2'}(\mathbf{q}')\mathcal{V}_{\lambda_2}(\mathbf{q})\Phi^{JPC\dagger}_{\lambda_1'\lambda_2'}(\mathbf{q}')\Phi^{JPC}_{\lambda_1\lambda_2}(\mathbf{q})\,, \tag{18}$$

with $\mathbf{p} = \mathbf{q} - \mathbf{q}'$ and $\mathbf{q}$, $\mathbf{q}'$ the initial and final quark momenta. The dressed spinors, $\mathcal{U}_\lambda, \mathcal{V}_\lambda$, are BCS rotations of the bare spinors, and details of the wavefunction are given in the following sections. The above integration is convergent and the numerical value for this Coulomb type interaction energy is $E_2^C = 25.6\,\mathrm{MeV}$.

The g^4 diagram reduces to

$$E_4^{\mathrm{C}} = \int \mathrm{d}\mathbf{q}\mathrm{d}\mathbf{q}'\,\mathrm{d}\mathbf{q}_1 \frac{4(1-x_1^2)\mathcal{F}(\mathbf{q},\mathbf{q}')}{\mathbf{p}^2(\mathbf{p}-\mathbf{q}_1)^2\omega(\mathbf{q}_1)}\,, \tag{19}$$

where $x_1 = \hat{\mathbf{p}}\cdot\hat{\mathbf{q}}_1$. The momentum integration $\mathbf{q}_1$ over the loop diverges but replacing the gluon kinetic energy $\omega(\mathbf{q}_1)$ with $\omega(\mathbf{q}_1)^{1+\epsilon}$ yields a finite result, $A + B/\epsilon$, for positive ϵ, which isolates the divergence. As shown in Fig. 2, the integrated value scales as $1/\epsilon$ for small ϵ, which is consistent with dimensional renormalization. Extrapolating the intercept from the linear graph yields the infinite subtracted renormalized result $E_4^{\mathrm{C}} = A = 13.2\,\mathrm{MeV}$. In this minimal subtraction scheme the coupling g is renormalized to its physical value by absorbing the infinity.

The bottom three diagrams of Fig. 1 (from left to right) are proportional to g^6, with respective expectation values

$$\int \mathrm{d}\mathbf{q}\mathrm{d}\mathbf{q}'\,\mathrm{d}\mathbf{q}_1\,\mathrm{d}\mathbf{q}_2 \frac{16\big(1-x_1^2\big)\big(1-x_2^2\big)\mathcal{F}(\mathbf{q},\mathbf{q}')}{\mathbf{p}^2(\mathbf{p}-\mathbf{q}_1)^2(\mathbf{p}-\mathbf{q}_2)^2\omega(\mathbf{q}_1)\omega(\mathbf{q}_2)}\,,$$
$$\int \mathrm{d}\mathbf{q}\mathrm{d}\mathbf{q}'\,\mathrm{d}\mathbf{q}_1 d\mathbf{q}_2 \frac{4(1-x_1^2)\mathbf{k}_1^2(1-z^2)\mathcal{F}(\mathbf{q},\mathbf{q}')}{\mathbf{p}^2(\mathbf{p}-\mathbf{q}_1)^4(\mathbf{p}-\mathbf{q}_1-\mathbf{q}_2)^2\omega(\mathbf{q}_1)\omega(\mathbf{q}_2)}\,,$$
$$\int \frac{\mathrm{d}\mathbf{q}\mathrm{d}\mathbf{q}'\,\mathrm{d}\mathbf{q}_1\,\mathrm{d}\mathbf{q}_2\mathcal{F}(\mathbf{q},\mathbf{q}')}{\mathbf{p}^4(\mathbf{p}-\mathbf{q}_1)^2(\mathbf{p}-\mathbf{q}_2)^2(\mathbf{p}-\mathbf{q}_1-\mathbf{q}_2)^2\omega(\mathbf{q}_1)\omega(\mathbf{q}_2)}$$
$$\times\big[\mathbf{k}_1\cdot(\mathbf{k}_1-2\mathbf{q}_2)-\mathbf{k}_1\cdot\mathbf{q}_1(\mathbf{k}_1-2\mathbf{q}_2)\cdot\mathbf{q}_1/\mathbf{q}_1^2\big]$$
$$\times\big[\mathbf{k}_2\cdot(\mathbf{k}_2-2\mathbf{q}_1)-\mathbf{k}_2\cdot\mathbf{q}_2(\mathbf{k}_2-2\mathbf{q}_1)\cdot\mathbf{q}_2/\mathbf{q}_2^2\big]\,,$$

where $z = \hat{\mathbf{k}}_1\cdot\hat{\mathbf{q}}_2$, $x_j = \hat{\mathbf{p}}\cdot\hat{\mathbf{q}}_j$ and $\mathbf{k}_j = 2\mathbf{p} - \mathbf{q}_j$ for $j = 1, 2$. These loop variable integrations are also divergent. Using the same renormalization procedure yields the respective values $7.15g^6$, $7.86g^6$ and $0.48g^6\,\mathrm{MeV}$. Therefore, the sixth order interaction energy is $E_6^{\mathrm{C}} = 15.5\,\mathrm{MeV}$ and the series takes the form $E_{\mathrm{C}} = (25.6g^2 + 13.2g^4 + 15.5g^6)\,\mathrm{MeV}$. Since the coefficients are comparable, g^2 must be less than 1, i.e. $\alpha_{\mathrm{s}} = g^2/4\pi < 0.1$, for perturbation theory to be valid but the strong interaction has α_{s} much larger, so the perturbative expansion fails, as anticipated. We therefore seek a calculable confining kernel interaction and, guided by lattice results, adopt a linear potential specified in the next section. We note in passing that a subset or class of diagrams may still be amendable to a perturbative treatment. Specifically the chain of bubble diagrams (i.e. the g^4 and first g^6 diagrams in Fig. 1) seems to be converging. Also, ladder type diagrams (third g^6 diagram) seem much smaller, in contrast to dressed gluon or self-energy type diagrams (second g^6 diagram), and they too may be convergent. Hence further perturbative studies should be conducted to determine which parts, if any, of the exact kernel can be treated as radiative corrections and which parts are responsible for confinement and must be included non-perturbatively. This would provide further insight into the nature of confinement and also for improved QCD approximated interactions.

4 Coulomb gauge model Hamiltonian

Our model's starting point is the Coulomb gauge QCD Hamiltonian, (1). In this gauge, the color form of Gauss's law, which is essential for confinement, is satisfied exactly

and can be used to eliminate the unphysical longitudinal gluon fields. We then make two approximations: 1) replace the exact Coulomb kernel with a calculable confining potential; 2) use the lowest order, unit value for the Faddeev–Popov determinant.

This defines the CG model Hamiltonian

$$H_{\rm CG} = H_q + H_g^{\rm CG} + H_{qg} + H_{\rm C}^{\rm CG}\,, \tag{20}$$

$$H_g^{\rm CG} = \frac{1}{2}\int {\rm d}\mathbf{x}\left[\mathbf{\Pi}^a(\mathbf{x})\cdot\mathbf{\Pi}^a(\mathbf{x}) + \mathbf{B}^a(\mathbf{x})\cdot\mathbf{B}^a(\mathbf{x})\right]\,, \tag{21}$$

$$H_{\rm C}^{\rm CG} = -\frac{1}{2}\int {\rm d}\mathbf{x}\,{\rm d}\mathbf{y}\rho^a(\mathbf{x})\hat{V}(|\mathbf{x}-\mathbf{y}|)\rho^a(\mathbf{y})\,. \tag{22}$$

Confinement is described by a kernel that is a Cornell type potential, $\hat{V}(r) = -\alpha_{\rm s}/r + \sigma r$, where the string tension, $\sigma = 0.135\ {\rm GeV}^2$, and $\alpha_{\rm s} = 0.4$ have been previously determined and set the scale for the calculation.

Next, hadron states are expressed as dressed quark (anti-quark) Fock operators, $B^\dagger_{\lambda_1 c_1}$ ($D^\dagger_{\lambda_2 c_2}$), acting on the Bardeen–Cooper–Schrieffer (BCS) model vacuum, $|\Omega\rangle$ [21, 23]. For the tetra-quark system, the quark (anti-quark) CM momenta are $\mathbf{q}_1$, $\mathbf{q}_3$ ($\mathbf{q}_2$, $\mathbf{q}_4$) and the following wave function ansatz is adopted:

$$|\Psi^{JPC}\rangle = \int \frac{{\rm d}\mathbf{q}_1}{(2\pi)^3}\frac{{\rm d}\mathbf{q}_2}{(2\pi)^3}\frac{{\rm d}\mathbf{q}_3}{(2\pi)^3}\Phi^{JPC}_{\lambda_1\lambda_2\lambda_3\lambda_4}(\mathbf{q}_1,\mathbf{q}_2,\mathbf{q}_3) \times R^{\mathcal{C}_1\mathcal{C}_2}_{\mathcal{C}_3\mathcal{C}_4} B^\dagger_{\lambda_1\mathcal{C}_1}(\mathbf{q}_1)D^\dagger_{\lambda_2\mathcal{C}_2}(\mathbf{q}_2)B^\dagger_{\lambda_3\mathcal{C}_3}(\mathbf{q}_3)D^\dagger_{\lambda_4\mathcal{C}_4}(\mathbf{q}_4)|\Omega\rangle\,. \tag{23}$$

The expression for the matrix $R^{\mathcal{C}_1\mathcal{C}_2}_{\mathcal{C}_3\mathcal{C}_4}$ depends on the specific color scheme selected [20, 22]. Here, we focus on the color singlet–singlet scheme, $[(3\otimes\bar{3})_1\otimes(3\otimes\bar{3})_1]_1$, where the $q\bar{q}$ pairs couple to color singlets, since it gives the lowest mass among the four color representations. This yields $R^{\mathcal{C}_1\mathcal{C}_2}_{\mathcal{C}_3\mathcal{C}_4} = \delta_{\mathcal{C}_1\mathcal{C}_2}\delta_{\mathcal{C}_3\mathcal{C}_4}$. The spin part of the wave function is

$$\left\langle \frac{1}{2}\frac{1}{2}\lambda_1\lambda_2\,|s_A\lambda_A\rangle \times \left\langle \frac{1}{2}\frac{1}{2}\lambda_3\lambda_4\middle| s_B\lambda_B\right\rangle \langle s_A s_B\lambda_A\lambda_B|\,J\lambda_A+\lambda_B\rangle\,,$$

a product of Clebsch–Gordan coefficients. Here J is the total angular momentum, $\mathbf{s}_A = \mathbf{s}_1 + \mathbf{s}_2$, $\mathbf{s}_B = \mathbf{s}_3 + \mathbf{s}_4$, and for scalar hadrons all orbital angular momenta, l_X, are zero, consistent with the lowest energy state (see Sect. 6 for p-wave pseudo-scalar and vector hadrons). A Gaussian radial wavefunction is used [22]:

$$f(q_A, q_B, q_I) = {\rm e}^{-\frac{q_A^2}{\alpha_A^2}-\frac{q_B^2}{\alpha_B^2}-\frac{q_I^2}{\alpha_I^2}}\,, \tag{24}$$

with variational parameters $\alpha_A = \alpha_B$ and α_I determined by minimizing the tetra-quark masses

$$M_{JPC} = \langle\Psi^{JPC}|H_{\rm CG}|\Psi^{JPC}\rangle = M_{\rm self} + M_{qq} + M_{\bar{q}\bar{q}} + M_{q\bar{q}} + M_{\rm annih}\,, \tag{25}$$

which were previously calculated [20, 22]. The subscripts indicate the source of each contribution: the q and $\bar{q}$ self-energy, qq, $\bar{q}\bar{q}$ and $q\bar{q}$ scattering, and $q\bar{q}$ annihilation, respectively. Finally, the $q\bar{q}$ meson state is

$$|\Psi^{JPC}\rangle = \int \frac{{\rm d}\mathbf{k}}{(2\pi)^3}\Phi^{JPC}_{\lambda_1\lambda_2}(\mathbf{k})B^\dagger_{\lambda_1}(\mathbf{k})D^\dagger_{\lambda_2}(-\mathbf{k})|\Omega\rangle\,. \tag{26}$$

5 Meson and tetra-quark mixing

In this section, we discuss the meson and tetra-quark mixing for the $J^{PC} = 0^{\pm+}$ and 1^{--} states. As discussed above, only mixing between flavored (u, d, s) $q\bar{q}$ mesons and tetra-quarks is investigated. Using the notation $|q\bar{q}\rangle$ and $|q\bar{q}q\bar{q}\rangle$ for $|\Psi^{JPC}\rangle$, the mixed state is given by

$$|J^{PC}\rangle = a|n\bar{n}\rangle + b|s\bar{s}\rangle + c|n\bar{n}n\bar{n}\rangle + d|n\bar{n}s\bar{s}\rangle\,, \tag{27}$$

where $n\bar{n} = \frac{1}{\sqrt{2}}(u\bar{u} + d\bar{d})$. The state $|s\bar{s}s\bar{s}\rangle$ is not included, since its mass is much higher than the meson masses. The coefficients a, b, c and d are determined by diagonalizing the Hamiltonian matrix, in which the meson–tetra-quark off-diagonal mixing element is (only $H_{\rm C}^{\rm CG}$ contributes)

$$M = \langle q\bar{q}|H_{\rm C}^{\rm CG}|q\bar{q}q\bar{q}\rangle\,, \tag{28}$$

where $|q\bar{q}\rangle$ is $|n\bar{n}\rangle$ or $|s\bar{s}\rangle$, and $|q\bar{q}q\bar{q}\rangle$ is $|n\bar{n}n\bar{n}\rangle$ or $|n\bar{n}s\bar{s}\rangle$. There are six off-diagonal matrix elements; however, two, $\langle s\bar{s}|H_{\rm C}^{\rm CG}|n\bar{n}\rangle$ and $\langle s\bar{s}|H_{\rm C}^{\rm CG}|n\bar{n}n\bar{n}\rangle$, vanish and one (see below), $\langle n\bar{n}n\bar{n}|H_{\rm C}^{\rm CG}|n\bar{n}s\bar{s}\rangle$, is computed and found to be very small. The remaining mixing matrix elements are $\langle n\bar{n}|H_{\rm C}^{\rm CG}|n\bar{n}n\bar{n}\rangle$, $\langle n\bar{n}|H_{\rm C}^{\rm CG}|n\bar{n}s\bar{s}\rangle$ and $\langle s\bar{s}|H_{\rm C}^{\rm CG}|n\bar{n}s\bar{s}\rangle$. For our model Hamiltonian, there are two types of mixing diagrams illustrated in Fig. 3. Because of color factors, nonzero mixing only exists for $q\bar{q}$ annihilation between different singlet $q\bar{q}$ clusters. The expression for the first diagram in Fig. 3 is

$$M_1 = \frac{1}{2}\int {\rm d}\mathbf{q}_1\,{\rm d}\mathbf{q}_2\,{\rm d}\mathbf{q}_3 V(k)\mathcal{U}^\dagger_{\lambda_1}(\mathbf{q}_1)\mathcal{U}_{\lambda_1'}(-\mathbf{q}_4) \times\mathcal{U}^\dagger_{\lambda_3}(\mathbf{q}_3)\mathcal{V}_{\lambda_2}(\mathbf{q}_2)\Phi^{JPC\dagger}_{\lambda_1\lambda_2\lambda_3\lambda_4}(\mathbf{q}_1,\mathbf{q}_2,\mathbf{q}_3)\Phi^{JPC}_{\lambda_1'\lambda_4}(-2\mathbf{q}_4)\,, \tag{29}$$

with $\mathbf{q}_4 = -\mathbf{q}_1 - \mathbf{k}$, $\mathbf{k} = \mathbf{q}_2 + \mathbf{q}_3$ and dressed, BCS spinors

$$\mathcal{U}_\lambda = \frac{1}{\sqrt{2}}\begin{pmatrix}\sqrt{1+\sin\phi(q)}\\ \sqrt{1-\sin\phi(q)}\sigma\cdot\hat{\mathbf{q}}\end{pmatrix}\chi_\lambda \tag{30}$$

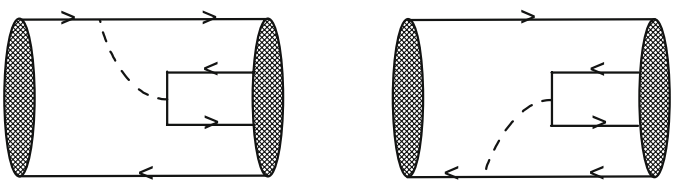

Fig. 3. Diagrams for the meson, tetra-quark mixing term

$$\mathcal{V}_\lambda = \frac{1}{\sqrt{2}} \begin{pmatrix} -\sqrt{1-\sin\phi(q)}\sigma\cdot\hat{\mathbf{q}} \\ \sqrt{1+\sin\phi(q)} \end{pmatrix} \chi_\lambda \,. \tag{31}$$

The gap angle, $\phi(q)$, is the solution to the gap equation that minimizes the energy of the BCS vacuum, i.e., the vacuum rotated by a Bogoliubov–Valatin transformation [23]. The effective confining potential in momentum space is $V(k)$. The second diagram in Fig. 3 yields

$$M_2 = \frac{1}{2}\int \mathrm{d}\mathbf{q}_1\,\mathrm{d}\mathbf{q}_2\,\mathrm{d}\mathbf{q}_3 V(k)\mathcal{V}^\dagger_{\lambda_4}(\mathbf{q}_4)\mathcal{V}_{\lambda'_4}(-\mathbf{q}_1) \times \mathcal{U}^\dagger_{\lambda_3}(\mathbf{q}_3)\mathcal{V}_{\lambda_2}(\mathbf{q}_2)\Phi^{JPC\dagger}_{\lambda_1\lambda_2\lambda_3\lambda_4}(\mathbf{q}_1,\mathbf{q}_2,\mathbf{q}_3)\Phi^{JPC}_{\lambda_1\lambda'_4}(2\mathbf{q}_1)\,. \tag{32}$$

6 Numerical results

The two Hamiltonian parameters in our model were independently determined, while the wavefunction parameters were obtained variationally. Because we seek new model masses, the unmixed variational basis states need not be ones producing a minimal, unmixed mass. Hence we can use one of the variational parameters to provide an optimal mixing prediction. We have selected α_I to exploit this freedom and studied the mixing sensitivity to this parameter.

The tetra-quark parity and charge parity are given by $P=(-1)^{l_A+l_B+l_I}$ and $C=(-1)^{l_A+s_A+l_B+s_B}$, so for the lightest, unmixed $J^{PC}=0^{\pm+}, 1^{--}$ states

$$\begin{aligned} 0^{++} &\quad l_A=l_B=l_I=0, s_A=s_B=0 \text{ or } s_A=s_B=1\,, \\ 0^{-+} &\quad l_A=l_B=0, l_I=1, s_A=s_B=1\,, \\ 1^{--} &\quad l_A=l_B=0, l_I=1, s_A=1 \text{ or } s_B=1\,. \end{aligned}$$

For the 1^{--} p-wave state we choose $l_I=1$, since this yields a lower mass than states with $l_A=1$ or $l_B=1$. Note for the 0^{++} state that the spin of the two $q\bar{q}$ clusters are both either 0 or 1 and for each the three mixing matrix elements versus α_I are shown in Fig. 4. The mixing term is zero when α_I is zero and then increases with increasing α_I. Also, mixing with $s\bar{s}$ states is stronger than with $n\bar{n}$ states. In particular, for $\alpha_I=0.2$, the $s_A=s_B=0$ matrix elements are $\langle s\bar{s}|H_{\mathrm{C}}^{\mathrm{CG}}|n\bar{n}s\bar{s}\rangle = 365\,\mathrm{MeV}$, $\langle n\bar{n}|H_{\mathrm{C}}^{\mathrm{CG}}|n\bar{n}n\bar{n}\rangle = 166\,\mathrm{MeV}$ and $\langle n\bar{n}|H_{\mathrm{C}}^{\mathrm{CG}}|n\bar{n}s\bar{s}\rangle = 45\,\mathrm{MeV}$.

Figure 5 shows the mixing versus α_I for the 0^{-+} states. Again, all mixing terms are zero for $\alpha_I=0$ and then increase with increasing α_I. In contrast to the 0^{++} result, $\langle n\bar{n}|H_{\mathrm{CG}}|n\bar{n}n\bar{n}\rangle$ now has the largest value. The value $\alpha_I=0.5$ yields reasonable η and η' masses with mixing elements $\langle n\bar{n}|H_{\mathrm{C}}^{\mathrm{CG}}|n\bar{n}n\bar{n}\rangle = 219\,\mathrm{MeV}$, $\langle n\bar{n}|H_{\mathrm{C}}^{\mathrm{CG}}|n\bar{n}s\bar{s}\rangle = 157\,\mathrm{MeV}$ and $\langle s\bar{s}|H_{\mathrm{C}}^{\mathrm{CG}}|n\bar{n}s\bar{s}\rangle = 138\,\mathrm{MeV}$.

For the 1^{--} states a novel mixing result was obtained. The mixing matrix elements were again 0 for $\alpha_I=0$, but, very interesting, also essentially 0 for all values of α_I. Our model therefore predicts minimal flavor mixing for vector mesons, which would explain the known ω/ϕ ideal mixing. Related with this is that weak mixing also provides a good description of the spectrum, since the pure $n\bar{n}$ and $s\bar{s}$ states were previously in good agreement [23, 24] with observation.

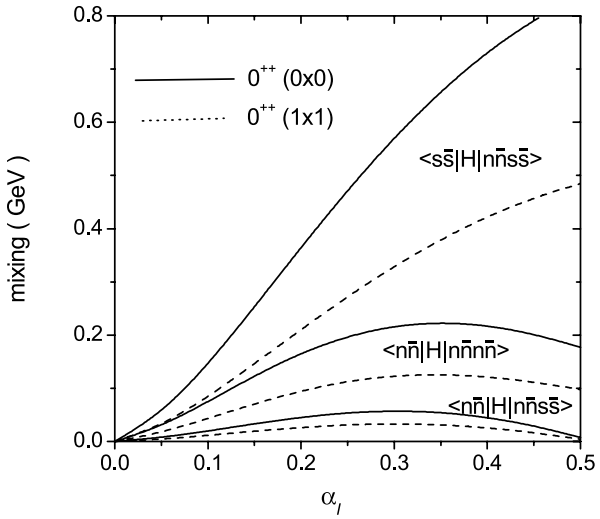

Fig. 4. The 0^{++} mixing matrix elements vs. α_I. *Solid* and *dashed lines* are for $q\bar{q}$ spin 0 and 1, respectively

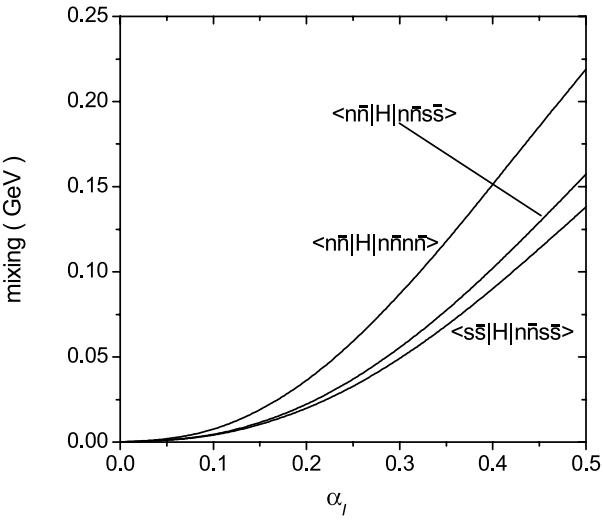

Fig. 5. The 0^{-+} mixing matrix elements vs. α_I

As mentioned above, the purely tetra-quark matrix element, $\langle n\bar{n}n\bar{n}|H_{\mathrm{CG}}|n\bar{n}s\bar{s}\rangle$, was calculated to be small, since only annihilation diagrams contribute. Its value was only a few MeV in magnitude for any α_I and thus has no appreciable effect in this study.

With the calculated matrix elements and previously predicted unmixed meson and tetra-quark masses [20, 22, 23], the complete Hamiltonian matrix was diagonalized to obtain the expansion coefficients and masses for the corresponding eigenstates. Using $\alpha_I=0.2$, the results for 0^{++} states are compared in Table 1 to the observed [1] lowest six 0^{++} states. Noteworthy, after mixing, the σ meson mass is shifted from 848 to 776 MeV and the strange scalar meson mass also decreases from 1297 MeV to 1006 MeV, now close to the experimental value of 980 MeV. Meson and tetra-quark mixing clearly improves the model predictions as the masses of the other f_0 states are also in better agreement with the data. Figure 6 illustrates the over-all improved de-

Table 1. Mixing coefficients and masses in MeV for 0^{++} states

	$\|n\bar{n}\rangle$	$\|s\bar{s}\rangle$	$\|n\bar{n}n\bar{n}\rangle_1$	$\|n\bar{n}n\bar{n}\rangle_2$	$\|n\bar{n}s\bar{s}\rangle_1$	$\|n\bar{n}s\bar{s}\rangle_2$
no mixing	848	1297	1282	1418	1582	1718
mixing	776	1006	1329	1440	1676	1918
exp.	$f_0(600)$	$f_0(980)$	$f_0(1370)$	$f_0(1500)$	$f_0(1710)$	$f_0(2020)$
	400–1200	980 ± 10	1200–1500	1507 ± 5	1718 ± 2	1992 ± 16
coeff.	a	b	c_1	c_2	d_1	d_2
$f_0(600)$	0.936	−0.075	0.263	0.216	0.030	−0.007
$f_0(980)$	0.057	0.818	−0.022	−0.017	0.549	−0.156
$f_0(1370)$	−0.308	0.045	0.922	0.228	0.008	−0.003
$f_0(1500)$	−0.139	0.017	−0.282	0.949	0.006	−0.003
$f_0(1710)$	−0.031	−0.240	−0.001	−0.002	0.582	0.776
$f_0(2020)$	−0.063	−0.514	−0.002	−0.006	0.599	−0.610

scription that mixing provides for the f_0 spectrum. New insight in the structure has also been obtained from the coefficients, with the predictions that $\sigma/f_0(600)$ is predominantly a mixture of $n\bar{n}$ and $n\bar{n}n\bar{n}$ states, while $f_0(980)$ consists mainly of $s\bar{s}$ and $n\bar{n}s\bar{s}$ states.

As concluded in previous studies [13, 18–20], a complete description of the scalar spectrum requires tetra-quark states. However, the degree of mixing remains unclear. References [18, 19] find that below 1 GeV tetra-quark states dominate, while [13] concludes differently and reports that $f_0(600)$ has only a 16% tetra-quark mixing component (note that they find that $f_0(980)$ has a 83% tetra-quark admixture). There is growing consensus [33] that the $\sigma/f_0(600)$ state is a $\pi\pi$ resonance (pole in the $\pi\pi$ scattering amplitude) and thus has a predominantly tetra-quark nature. Because the current numerical treatment of our CG model neglects chiral symmetry, our mass predictions for tetra-quark states, which couple to the $\pi\pi$ quantum numbers, will generally be too heavy and should be regarded as preliminary. A chiral symmetry preserving RPA variational mixing study will be conducted in the future that should yield a lighter scalar tetra-quark mass, since our approach is formally equivalent to the Schwinger–Dyson treatment that previously predicted that σ is a $\pi\pi$ resonance [28, 29]. A subsequent, similar mixing analysis should then modify and further improve our predicted low-lying f_0 spectrum.

Table 2 lists the masses and coefficients for the 0^{-+} states for $\alpha_I = 0.5$. Again, mixing lowers (raises) the predicted mass for states relative to unmixed $q\bar{q}$ ($q\bar{q}q\bar{q}$) states. All mixed hadron masses are closer to measurement than the unmixed ones, except the most massive state, which presumably could further mix with omitted heavier configurations. Note from the expansion coefficients that flavor mixing is again weak (i.e. $n\bar{n}$ with $s\bar{s}$) and less likely than meson, tetra-quark mixing having the same flavors.

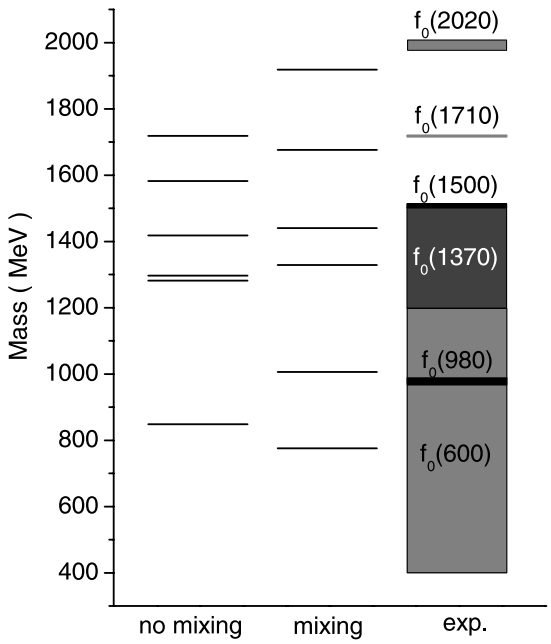

Fig. 6. Unmixed and mixed f_0 spectrum compared to data

7 Summary and conclusions

We have applied the established CG model to study $q\bar{q}$ and $q\bar{q}q\bar{q}$ mixing for the low-lying 0^{++}, 0^{-+} and 1^{--} spectra. In general, mixing effects are significant and provide an improved hadronic description. As important is that our findings clearly document that mixing is necessary for a complete understanding of scalar and pseudo-scalar hadrons.

The mixed 0^{++} states are a superposition of six states with coefficients obtained by diagonalizing the $H_{\rm CG}$ Hamiltonian, which decreases the mass for states dominated by $q\bar{q}$ components, while increasing those predominantly having tetra-quark configurations. The resulting f_0 mass spectrum is in good agreement with observation.

Mixing is not as large for the 0^{-+} spectrum; therefore, the mass shifts are smaller. Again after mixing, predominantly $q\bar{q}q\bar{q}$ states increase in mass, while the $q\bar{q}$ dominated masses decrease. All mixed states are closer to measurement except the heaviest that might be further corrected via mixing with the omitted higher configurations. It is noteworthy that the CG model provides sufficient flavor

Table 2. Mixing coefficients and masses in MeV for 0^{-+} states

	$n\bar{n}$	$s\bar{s}$	$\|n\bar{n}n\bar{n}\rangle$	$\|n\bar{n}s\bar{s}\rangle$
no mixing	610	1002	1252	1552
mixing	531	970	1316	1598
exp.	η	η'	$\eta(1295)$	$\eta(1405)$
	547.51 ± 0.18	957.78 ± 0.14	1294 ± 4	1409.8 ± 2.5
coeff.	a	b	c	d
η	0.951	–0.046	0.279	0.126
η'	0.032	0.973	–0.046	0.223
$\eta(1295)$	–0.289	0.036	0.953	0.080
$\eta(1405)$	–0.108	–0.222	–0.105	0.963

mixing to produce reasonable masses for the historically challenging η, η' system.

Significantly, mixing is calculated to be weak for the 1^{--} states. Therefore, minimal flavor mixing for vector mesons follows naturally from our model, consistent with the known ω/ϕ ideal mixing.

Finally, we performed a perturbative investigation of the exact QCD Coulomb gauge kernel to order g^6. As expected, a series expansion in g does not converge; however, a subset class of diagrams might be amendable to a perturbative treatment and further study is recommended. Future work should also address the mixing applications to the other $I^G(J^{PC})$ states, especially glueball and hybrid mesons with explicit gluonic degrees of freedom. Determining the level of mixing for these exotic systems will be important for finally establishing their existence.

Acknowledgements. The authors are very appreciative for the assistance and advice from F. J. Llanes-Estrada. Supported in part by U.S. DOE grants DE-FG02-97ER41048 and DE-FG02-03ER41260.

References

1. W.-M. Yao et al., J. Phys. G **33**, 1 (2006)
2. Y.A. Simonov, Phys. Atom. Nucl. **64**, 1876 (2001)
3. N. Kochelev, D.-P. Min, Phys. Rev. D **72**, 097 502 (2005)
4. W.-J. Lee, D. Weingarten, Phys. Rev. D **61**, 014 015 (2000)
5. F. Giacosa, T. Gutsche, V.E. Lyubovitskij, A. Faessler, Phys. Rev. D **72**, 094 006 (2005)
6. L. Burakovsky, P.R. Page, Eur. Phys. J. C **12**, 489 (2000)
7. L.S. Celenza, B. Huang, H.S. Wang, C.M. Shakin, Brooklyn College Report No. BCCNT 99/111/283
8. F.E. Close, A. Kirk, Phys. Lett. B **483**, 345 (2000)
9. D.M. Li, H. Yu, Q.-X. Shen, Commun. Theor. Phys. **34**, 507 (2000)
10. X.-G. He, X.-Q. Li, X. Liu, X.-Q. Zeng, Phys. Rev. D **73**, 051 502(R) (2006)
11. X.-G. He, X.-Q. Li, X. Liu, X.-Q. Zeng, Phys. Rev. D **73**, 114 026 (2006)
12. H. Noya, H. Nakamura, Nucl. Phys. A **692**, 348c (2001)
13. F. Giacosa, Phys. Rev. D **75**, 054 007 (2007)
14. E. van Beveren, G. Rupp, T.A. Rijken, C. Dullemond, Phys. Rev. D **27**, 1527 (1983)
15. E. van Beveren, T.A. Rijken, K. Metzger, C. Dullemond, G. Rupp, J.E. Ribeiro, Z. Phys. C **30**, 615 (1986)
16. B. Silvestre-Brac, J. Vijande, F. Fernandez, A. Valcarce, AIP Conf. Proc. **814**, 665 (2006)
17. D. Black, A.H. Fariborz, F. Sannino, J. Schechter, Phys. Rev. D **59**, 074 026 (1999)
18. D. Black, A.H. Fariborz, J. Schechter, Phys. Rev. D **61**, 074 001 (2000)
19. G. 't Hooft, G. Isidori, L. Maiani, A.D. Polosa, V. Riquer, arXiv:0801.2288 [hep-ph]
20. S.R. Cotanch, I.J. General, P. Wang, Eur. Phys. J. A **31**, 656 (2007)
21. I.J. General, S.R. Cotanch, F.J. Llanes-Estrada, Eur. Phys. J. C **51**, 347 (2007) [arXiv:hep-ph/0609115]
22. I.J. General, P. Wang, S.R. Cotanch, F.J. Llanes-Estrada, Phys. Lett. B **653**, 216 (2007) [arXiv:0707.1286]
23. F.J. Llanes-Estrada, S.R. Cotanch, Nucl. Phys. A **697**, 303 (2002)
24. F.J. Llanes-Estrada, S.R. Cotanch, A.P. Szczepaniak, E.S. Swanson, Phys. Rev. C **70**, 035 202 (2004)
25. F.J. Llanes-Estrada, P. Bicudo, S.R. Cotanch, Phys. Rev. Lett. **96**, 081 601 (2006)
26. F.J. Llanes-Estrada, S.R. Cotanch, Phys. Rev. Lett. **84**, 1102 (2000)
27. F.J. Llanes-Estrada, S.R. Cotanch, Phys. Lett. B **504**, 15 (2001)
28. S.R. Cotanch, P. Maris, Phys. Rev. D **66**, 116 010 (2002)
29. S.R. Cotanch, P. Maris, Phys. Rev. D **68**, 036 006 (2003)
30. P. Bicudo, S.R. Cotanch, F.J. Llanes-Estrada, D.G. Robertson, Eur. Phys. J. C **52**, 363 (2007)
31. T.D. Lee, Particle Physics and Introduction to Field Theory (Harwood Academic Publishers, New York, 1990)
32. D. Zwanziger, Nucl. Phys. B **485**, 185 (1997)
33. S.R. Cotanch, I.J. General, P. Wang, F.J. Llanes-Estrada, AIP Conf. Proc. Int. Workshop on Scalar Hadrons, Lisbon, Portugal (2008), to be published